INTERFACE

royalsocietypublishing.org/journal/rsif

Research

Cite this article: Chaudhary G, Ewoldt RH, Thiffeault J-L. 2019 Unravelling hagfish slime. *J. R. Soc. Interface* **16**: 20180710.
http://dx.doi.org/10.1098/rsif.2018.0710

Received: 21 September 2018
Accepted: 20 December 2018

Subject Category:
Life Sciences–Physics interface

Subject Areas:
biomaterials, biomechanics, biophysics

Author for correspondence:
Randy H. Ewoldt
e-mail: ewoldt@illinois.edu

Electronic supplementary material is available online at https://dx.doi.org/10.6084/m9.figshare.c.4356998.

THE ROYAL SOCIETY PUBLISHING

Unravelling hagfish slime

Gaurav Chaudhary[1], Randy H. Ewoldt[1] and Jean-Luc Thiffeault[2]

[1]Department of Mechanical Science and Engineering, University of Illinois at Urbana-Champaign, Urbana, IL, USA
[2]Department of Mathematics, University of Wisconsin, Madison, WI, USA

GC, 0000-0002-5428-5094; RHE, 0000-0003-2720-9712; J-LT, 0000-0001-7724-7966

Hagfish slime is a unique predator defence material containing a network of long fibrous threads each ~10 cm in length. Hagfish release the threads in a condensed coiled state known as skeins (~100 µm), which must unravel within a fraction of a second to thwart a predator attack. Here we consider the hypothesis that viscous hydrodynamics can be responsible for this rapid unravelling, as opposed to chemical reaction kinetics alone. Our main conclusion is that, under reasonable physiological conditions, unravelling due to viscous drag can occur within a few hundred milliseconds, and is accelerated if the skein is pinned at a surface such as the mouth of a predator. We model a single skein unspooling as the fibre peels away due to viscous drag. We capture essential features by considering simplified cases of physiologically relevant flows and one-dimensional scenarios where the fibre is aligned with streamlines in either uniform or uniaxial extensional flow. The peeling resistance is modelled with a power-law dependence on peeling velocity. A dimensionless ratio of viscous drag to peeling resistance appears in the dynamical equations and determines the unraveling time scale. Our modelling approach is general and can be refined with future experimental measurements of peel strength for skein unravelling. It provides key insights into the unravelling process, offers potential answers to lingering questions about slime formation from threads and mucous vesicles, and will aid the growing interest in engineering similar bioinspired material systems.

1. Introduction

Marine organisms present numerous interesting examples of fluid–structure interactions that are necessary for their physiological functions such as feeding [1,2], motion [3], mechanosensing [4] and defence [5]. A rather remarkable and unusual example of fluid–structure interaction is the production of hagfish slime, also known as hagfish defence gel. The hagfish is an eel-shaped deep-sea creature that produces the slime when it is provoked [6]. Slime is formed from a small amount of biomaterial ejected from the hagfish's slime glands into the surrounding water [7]. The biomaterial expands by a factor of 10 000 (by volume) into a mucus-like cohesive mass, which is hypothesized to choke predators and thus provide defence against attacks (figure 1*a*) [8]. Such defence mechanisms have been observed in several species of hagfish [8,9].

The secreted biomaterial has two main constituents—gland mucus cells and gland thread cells—responsible for the mucus and fibrous component of slime, respectively [6,10]. The plasma membranes of both kinds of cells shear off when secreted from the slime glands [10,11]. In the present study, we focus on the secreted thread cells, referred to as skeins from here on. Skeins possess a remarkable structure wherein a long filament (10–16 cm in length) is efficiently packed in canonical loops into a prolate spheroid (120–150 µm by 50–60 µm) [7,10] (figure 1*b*). When mixed with the surrounding water, the fibre (1–3 µm thread diameter) unravels from the skein (figure 1*c*) and forms a fibrous network with other threads and mucous vesicles. This process occurs on time scales of a predator attack (100–400 ms), as apparent from video evidence [8,12].

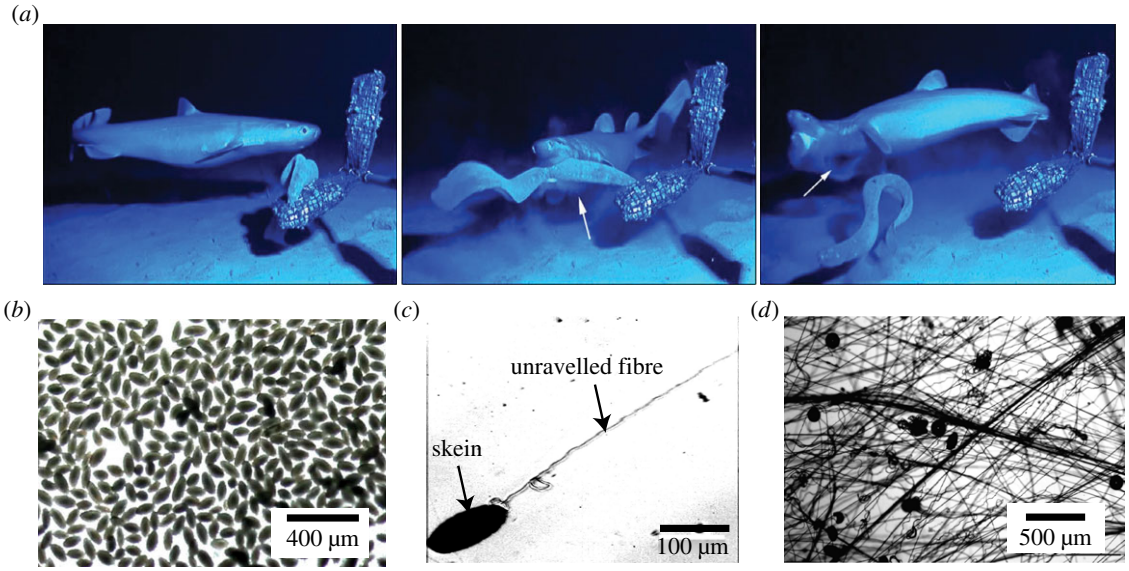

Figure 1. Slime defends hagfish against predator attacks. (*a*) Sequence of events during a predator attack (adapted from Zintzen *et al.* [8]). On being attacked, the hagfish produces a large quantity of slime that chokes the predator. The process of secretion and slime creation took less than 0.4 s. (*b*) Slime is formed from the secreted biomaterial, in part containing prolate-shaped skeins. (*c*) A skein unravels under the hydrodynamic forces from the surrounding flow field and produces a micrometre-width fibre of length 10–15 cm. (*d*) The unravelled fibres and mucous vesicles entrain a large volume of water to form a cohesive network. Details on materials and microscopy are provided in the electronic supplementary material, section I. (Online version in colour.)

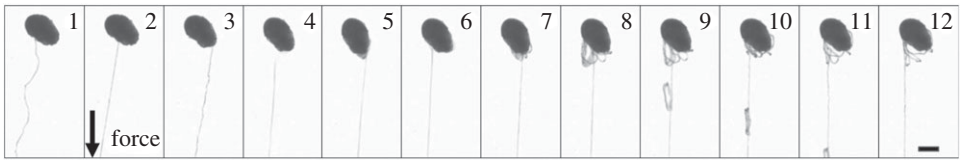

Figure 2. Unravelling a thread skein by pulling, as viewed with brightfield microscopy. Bottom right scale bar 50 µm.

While several studies have revealed the mechanical and biochemical aspects [13–17] of slime, little is known about the mechanisms involved in its rapid deployment. More recently, efforts have been made to understand the mechano-chemical aspects of the mucus component, and its swelling and rupture [18,19], but such an approach is yet to be extended to the mechano-chemical processes in the unravelling of skeins. Newby [20] postulated that the fibre is coiled under a considerable pressure and the rupture of the cell membrane allows the fibre to uncoil. However, later studies [12,21,22] have shown that convective mixing is essential for the production of fibres and slime. More recently, Bernards *et al.* [11] experimentally demonstrated that Pacific hagfish skeins can unravel even in the absence of flow, potentially due to chemical release of the adhesives holding the fibre together, but the time scales observed in their work are orders of magnitude larger than physiological time scales during the attack. Therefore, the key question about the fast time scales involved in this process remains to be answered. Deeper insights into the remarkable process of slime formation will aid the development of bioinspired material systems with novel functionality, such as materials with fast autonomous expansion and deployment. Motivated by the aforementioned experimental studies, our objective in this paper is to investigate the role of viscous hydrodynamics in skein unravelling via a simple physical model, and thus supply a qualitative understanding of the unravelling process.

The key question we answer here is whether the viscous hydrodynamic unravelling alone can account for the fast unravelling time scales that are observed in physiological scenarios. We hypothesize that suction feeding in marine predators creates sufficient hydrodynamic stresses to aid in the unravelling of skeins and set up the slime network. We develop fundamental insight by considering only the simplest flow fields—uniform flow and extensional flow. Our modelling framework, however, generalizes to complex flow fields that occur in physiological conditions.

In §2, we present a simple qualitative experiment demonstrating the force-induced unravelling of a hagfish skein. This motivates the model paradigm that follows. Section 3 outlines the problem statement, and we derive the general governing equations. In §4, the equations are solved for skein unravelling in simple flows under different physically relevant scenarios. In §5, we discuss the results in more detail, including the influence of constitutive model parameters for the peel strength, and comment on the qualitative comparisons between the experimental studies and theoretical work.

2. Unravelling experiment

To motivate the mathematical modelling, we perform a simple experiment demonstrating the force-induced unravelling of thread from a skein (figure 2; see also electronic supplementary material, video). A skein, obtained from Atlantic hagfish, is held in place by weak interactions with the substrate, and a force is applied to the dangling end using a syringe tip that

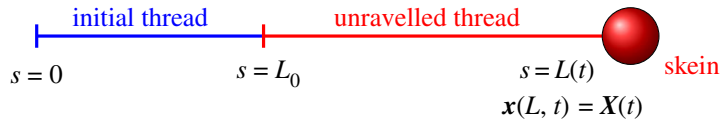

Figure 3. Simplified model of thread being drawn from a skein. The thread has length $L(t)$ with initial length $L(0) = L_0$. Here s is the arclength material (Lagrangian) coordinate along the unravelled thread, with $0 \leq s \leq L(t)$. The fixed laboratory (Eulerian) coordinate of the thread is $\boldsymbol{x}(s, t)$, with the thread peeling from the skein at $\boldsymbol{x}(L(t), t) = \boldsymbol{X}(t)$. (Online version in colour.)

naturally sticks to the filament. Figure 2 shows the unravelling skein at different time frames. Frame 1 shows the unforced and stable configuration, with no unravelling. Unravelling occurs only when a force is applied from frame 2 onwards. There are events when the thread peels away in clumps, but the orderly unravelling recovers quickly. A minimum peeling force seems required to unravel the thread from the skein. A simple estimate of the minimum peeling force based on weak adhesion (van der Waals interaction) between unravelling fibre and skein gives an estimate of 0.1 μN (see electronic supplementary material, section II).

3. Problem formulation

To determine if viscous hydrodynamic forces can account for fast skein unravelling, we consider a model of an inextensible slender thread unravelling from a spherical skein. The thread unravels and separates from the skein in response to a local force due to a viscous fluid flow surrounding the connected thread and skein. A schematic is shown in figure 3. Here $\boldsymbol{x}(s, t)$ is the Eulerian (laboratory) coordinate of the centreline of the filament as a function of the Lagrangian (material) thread arclength s, $0 \leq s \leq L(t)$, with $L(t)$ the time-dependent unravelled thread length. The thread is peeling from the skein at the Eulerian point $\boldsymbol{x}(L(t), t) = \boldsymbol{X}(t)$, which may depend on time if the skein is allowed to move.

3.1. Hydrodynamic force balance

We assume inertial effects, filament self-interactions, and external Brownian and gravitational forces to be negligible. The fluid dynamics in this situation are described by the Stokes equations. For the most general case of a thread in viscous flow, a local balance of filament forces and viscous forces (using local drag theory for a slender filament) is given by Tornberg & Shelley [23]

$$8\pi\mu\,\delta\,(\boldsymbol{x}_t - \boldsymbol{u}(\boldsymbol{x}, t)) = -((1+2\delta)\,\mathbb{I} + (1-2\delta)\,\hat{\boldsymbol{s}}\hat{\boldsymbol{s}})\cdot\boldsymbol{f}. \tag{3.1}$$

Here the tangent to the thread is $\hat{\boldsymbol{s}}$, the dynamic viscosity is μ and

$$\delta = -\frac{1}{\log(\varepsilon^2 \mathrm{e})} > 0, \quad \text{with } \varepsilon = \frac{r}{L}, \tag{3.2}$$

are the slenderness parameter and thread aspect ratio, respectively, with r the thread radius.

The internal net force per unit length, $\boldsymbol{f}$, of an inextensible filament is expressed by the Euler–Bernoulli bending theory for an elastic beam, and has both tensile and bending components,

$$\boldsymbol{f}(s) = -(T\boldsymbol{x}_s)_s + E\boldsymbol{x}_{ssss}, \quad |\boldsymbol{x}_s| = 1. \tag{3.3}$$

Here E is the bending modulus of the thread, $T(s, t)$ is the tension in the filament, and each subscript s denotes one derivative, e.g. $\boldsymbol{x}_s = \partial\boldsymbol{x}/\partial s$. The inextensibility condition is $|\boldsymbol{x}_s| = 1$, so s and distance along the thread must always coincide.

In the spirit of rheology, we consider the response to simple flows to isolate key features of the complex behaviour, obtain analytical results and gain an understanding of the unravelling process. We only consider cases with zero curvature, $\boldsymbol{x}_{ss} = 0$, immersed in one-dimensional flow fields, with the thread aligned with the flow streamlines. Equation (3.1) then reduces to a one-dimensional statement that the component of internal net filament force per unit length $f(s)$ along the streamline (taken as the x direction) is equal to the local viscous drag per unit length,

$$4\pi\mu\,\delta\,(x_t - u(x, t)) = -f. \tag{3.4}$$

Then the one-dimensional form of equation (3.3) with $x_{ssss} = 0$ and the inextensibility condition $x_s = 1$ gives $f = -T_s$, so that

$$T_s = 4\pi\mu\,\delta\,(x_t - u(x, t)). \tag{3.5}$$

With $x_s = 1$ and $x(L, t) = X(t)$ we have $x = X - L + s$, where X is the skein position, and thus $x_t = \dot{X} - \dot{L}$. We integrate (3.5) from $s = 0$ to L to find

$$T|_{s=L} - T|_{s=0} = 4\pi\mu L\,\delta\,(\dot{X} - \dot{L} - \frac{1}{L}\int_0^L u(X - L + s, t)\,\mathrm{d}s). \tag{3.6}$$

We then change the integration variable to $x = X - L + s$, and finally obtain

$$T_L - T_0 = -4\pi\mu L\,\delta\,(\dot{L} - \dot{X} + \bar{u}(L, X, t)), \tag{3.7}$$

where $T_L = T|_{s=L}$, $T_0 = T|_{s=0}$ and $\bar{u}(L, X, t)$ is the average velocity on the filament,

$$\bar{u}(L, X, t) := \frac{1}{L}\int_{X-L}^{X} u(x, t)\,\mathrm{d}x. \tag{3.8}$$

Equation (3.7) expresses the balance between the tension forces at the end of the thread and the drag force on the thread. We shall use this equation to derive a peeling formula for different thread–skein configurations in §4. But first, we need to examine how the thread will peel from the skein to unravel.

3.2. Unravelling from the skein

The relationship between R and L, respectively, the radius of the spherical skein and the length of the unravelled thread, is described by volume conservation

$$\frac{\mathrm{d}}{\mathrm{d}t}(\frac{4}{3}\pi\eta R^3 + \pi r^2 L) = 0 \Longrightarrow \dot{L} = -4\eta R^2\dot{R}/r^2. \tag{3.9}$$

Here r is the thread radius and $0 < \eta \leq 1$ is the packing fraction of thread into the spherical skein, assumed independent of R. (In this section, we keep the packing fraction as a variable, but in all later numerical simulations we take $\eta = 1$, since the skein is fairly tightly packed.) Explicitly,

we have

$$R^3 = R_0^3 - \frac{3}{4}(L - L_0)r^2/\eta \tag{3.10}$$

with R_0 the initial skein radius and L_0 the initial unravelled length. A convenient way of relating R and L is

$$R = R_0\left(\frac{L_{\max} - L}{L_{\max} - L_0}\right)^{1/3} \quad \text{and} \quad L_{\max} := L_0 + \frac{4}{3}\eta R_0^3/r^2, \tag{3.11}$$

where $L_{\max}$ is the total length of thread that can be extracted and L_0 is the initial unravelled length.

Next, we use a modified form of the work-energy theorem [24] to describe the unravelling dynamics,

$$\dot{E}_{\text{total}} = (T_L - F_{\text{P}}(V))\,V, \quad V = \dot{L}, \tag{3.12}$$

where $\dot{E}_{\text{total}}$ is the rate of change in total energy of the system, T_L is the net force (given by equation (3.7)) drawing out the thread at a peeling velocity V, and $F_{\text{P}}(V)$ is a velocity-dependent peeling force acting at the peeling site. Neglecting the inertia and changes to the elastic energy of the peeling thread gives

$$T_L = F_{\text{P}}(V), \quad V = \dot{L}. \tag{3.13}$$

A natural dimensionless quantity that will determine the dynamics of the unravelling process is given by the ratio of the net viscous drag force on the thread and the resisting peel force, each of which depends on a characteristic velocity U,

$$\wp := \frac{F_{\text{D}}(U)}{F_{\text{P}}(U)}. \tag{3.14}$$

The functional form of the peeling force, $F_{\text{P}}(V)$, in general, is dependent on parameters such as the chemistry of peeling surfaces, velocity of peeling, etc. In the absence of a known functional form for hagfish thread peeling, we use a simple constitutive form of peeling force that includes a wide range of behaviour, given by

$$F_{\text{P}}(V) = \alpha V^m, \quad 0 \le m \le 1, \tag{3.15}$$

for constant $\alpha > 0$ and m. Such a power-law form of peeling force has been observed in several engineered and biological systems [25–29]. Several other parametric forms of velocity-dependent peeling force exist that are functionally more complex [30,31]. However, to obtain simple and insightful solutions, we use the power-law form defined above. The form (3.15) allows for the limiting case $m = 0$, a constant peeling force, e.g. to simply counteract van der Waals attractions at the peel site.

For $m > 0$, we can rearrange equation (3.13) for the velocity, $V = \dot{L} = (T_L/\alpha)^{1/m}$. Using (3.9), we can then obtain a solution for the case where the tension at the peeling point, T_L, is constant,

$$\frac{4}{3}(R_0^3 - R^3) = \left(\frac{T_L}{\alpha}\right)^{1/m}\frac{r^2 t}{\eta}, \tag{3.16}$$

where $R_0 = R(0)$. From (3.16), we can easily extract the 'depletion time' or 'full-unravelling time' t_{dep} by setting $R = 0$,

$$t_{\text{dep}} = \frac{4\eta R_0^3}{3r^2}\left(\frac{T_L}{\alpha}\right)^{-1/m}. \tag{3.17}$$

In the next section, we compute this time scale when the skeins are subjected to different hydrodynamic flow scenarios, which cause different time histories of tension, $T_L(t)$.

4. Skein in one-dimensional flow

Having described the unravelling dynamics in §3.2 for the case of constant tension, T_L, we now consider a skein in a hydrodynamic flow where generally T_L varies in time as the thread–skein geometry changes during unravelling. In physiological scenarios the flow can arise from the hagfish–predator motion, or the suction feeding of the predator, or a combination of both. To simplify the problem we assume an incompressible flow of the form

$$\boldsymbol{u}(x, y, t) = (u(x, t), \; -yu_x(x, t)). \tag{4.1}$$

The thread will be assumed to lie along the x-axis. We solve for the depletion time for four relevant cases: pinned thread in uniform flow (§4.1); pinned skein in uniform flow (§4.2); free skein and thread in extensional flow (§4.3); and free skein splitting into two smaller skeins in extensional flow (§4.4).

4.1. Pinned thread

The simplest case to consider is the thread pinned at $s = 0$ in figure 3, with a uniform flow to the right, $u(x, t) = U$. This situation can arise in a controlled experiment if the thread is pinned down, or in the physiological unravelling process if the end of the thread is caught in the network of other threads, or stuck on the mouth of a predator.

The tension in the thread at $s = L$ balances the Stokes drag on the skein of radius R, $T_L = T(L(t), t) = 6\pi\mu R\,(u(L, t) - \dot{L})$. Using (3.13) and (3.15), we obtain the governing equation for unravelling as

$$(\dot{L})^m = 6\pi\mu\alpha^{-1}R(L)\,(u(L, t) - \dot{L}). \tag{4.2}$$

From (3.9), since $\dot{L} > 0$ (the thread never 're-spools'), the unspooling speed satisfies $\dot{L} \le u(L, t)$, i.e. the thread cannot unspool faster than the ambient flow speed. The radius $R(L)$ is given by (3.10).

We non-dimensionalize (4.2) using a characteristic length scale R_0 and flow speed U, which gives

$$(\dot{L}^*)^m = \wp\, R^*(L^*)\,(u^*(L^*, t^*) - \dot{L}^*), \tag{4.3}$$

where $\dot{L}^* = \dot{L}/U$, $R^* = R/R_0$ and $u^*(L^*, t^*) = u(L, t)/U$ are the non-dimensional unravelling rate, skein radius and flow rate, respectively. The non-dimensional time scale naturally results from these choices as $t^* = t/(R_0/U)$. The dimensionless quantity $\wp$ on the right-hand side of (4.3) is given by

$$\wp = \frac{6\pi\mu R_0\, U}{\alpha U^m} = 6\pi\mu R_0\, U^{1-m}\alpha^{-1}. \tag{4.4}$$

This is the ratio of characteristic drag to peeling force, as defined in (3.14). If $\wp$ is large (e.g. zero resistance to peeling), then (4.2) implies $\dot{L} \approx u(L, t)$, that is, in this drag-dominated limit, the drag force so easily unravels the skein that it advects with the local flow velocity. In the opposite limit of small $\wp$, we get $\dot{L} \approx 0$ and the skein cannot unravel. Hence, we require $\wp \gg 1$ for a fast unravel time.

To achieve the criterion $\wp \gg 1$, at a flow of speed $U = 1\ \text{m s}^{-1}$ and a skein of initial radius $R_0 = 50\ \mu\text{m}$, we require the peeling resistance at this velocity to satisfy $F_{\text{P}}(1\ \text{m s}^{-1}) \ll 1.4 \times 10^{-6}\ \text{N}$. The estimated van der Waals peeling force is much lower than this threshold, $F_{\text{vdW}} \sim 0.1\ \mu\text{N}$. At such a flow speed a skein containing 16.7 cm of thread (an upper bound physiological value) will unravel affinely (kinematically matching the flow speed) in roughly 167 ms. This lower bound

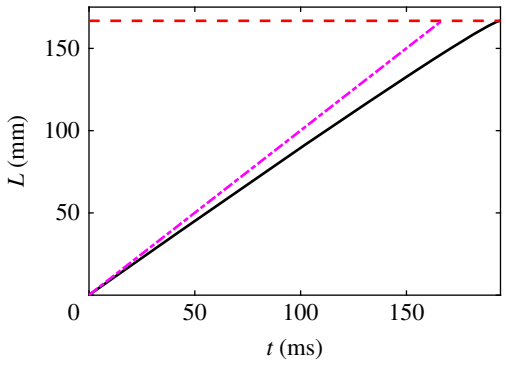

Figure 4. Numerical solution (solid line) of (4.2) for the parameter values $R_0 = 50\ \mu\text{m}$, $L_0 = 2R_0$, $\wp = 10$, $m = 1/2$, $U = 1\ \text{m s}^{-1}$. The dashed line (purple) is the upper bound $L = L_0 + Ut$. The horizontal dashed line is at $L = L_{\max}$, when the skein is fully unravelled. Even for such a moderate force ratio $\wp = 10$ the thread unravels almost as fast as the upper bound. (Online version in colour.)

estimate is commensurate with the rapidity with which hagfish slime is created (100–400 ms).

In figure 4, we show a numerical solution of (4.2) with a uniform flow for some typical physical parameter values, and assuming a moderately large force ratio $\wp = 10$. (Equation (4.2) is an implicit relation for $\dot{L}$ which must be solved numerically at every time step; it is a differential–algebraic equation rather than a simple ODE [30].) For these parameters, the kinematic lower bound on the depletion time is $L_{\max}/U \approx 167$ ms, and the numerical value is $t_{\text{dep}} \approx 194$ ms.

There is a mathematical oddity where the skein might not get depleted in finite time, depending on the exponent m. To see this, consider a skein close to depletion, $L = L_{\max} - U\tau$, where $\tau > 0$ is small. The equation for τ is

$$(-\dot{\tau})^m = \wp\left(\frac{U\tau}{L_{\max} - L_0}\right)^{1/3}(1 + \dot{\tau}), \quad \dot{\tau} < 0. \tag{4.5}$$

Since τ is small and we expect the thread to be drawn out slowly as it is almost exhausted, we take $1 + \dot{\tau} \approx 1$. Hence, we have the approximate form

$$(-\dot{\tau})^m \approx \mathrm{C}^m\,\tau^{1/3}, \quad \mathrm{C}^m := \wp\left(\frac{U}{(L_{\max} - L_0)}\right)^{1/3} \tag{4.6}$$

for some constant $\mathrm{C} > 0$, with solution

$$\tau(t) \approx \left[\tau_0^{1-1/3m} - \left(1 - \frac{1}{3m}\right)\mathrm{C}\,t\right]^{3m/(3m-1)}. \tag{4.7}$$

The behaviour of this solution as the skein is almost depleted depends on m. For $m > 1/3$, the exponent $3m/(3m-1)$ in (4.7) is greater than 1, so $\tau(t) \to 0$ as t approaches the depletion time, with $\tau'(t_{\text{dep}}) = 0$ so that $L(t)$ has slope zero when the skein is depleted (as can be seen at the very end in figure 4). We can thus rewrite (4.7) as

$$\tau(t) \approx \left[\left(1 - \frac{1}{3m}\right)\mathrm{C}\,(t_{\text{dep}} - t)\right]^{3m/(3m-1)}, \quad m > \frac{1}{3},\ t \nearrow t_{\text{dep}}. \tag{4.8}$$

For $m < 1/3$, the exponent $3m/(3m-1)$ is negative, but the factor $1 - 1/3m$ inside the brackets is also negative, so that $\tau(t)$ asymptotes to zero as $t \to \infty$ and the skein never gets fully depleted. In that case, we write (4.7) as

$$\tau(t) \approx \left[\left(\frac{1}{3m} - 1\right)\mathrm{C}t\right]^{-3m/(1-3m)}, \quad m < \frac{1}{3},\ t \to \infty. \tag{4.9}$$

Physically, for $m < 1/3$ the drag force ($\sim\tau^{1/3}$) is decreasing faster than the peeling force ($\sim\dot{\tau}^m$).

In practice, it is difficult to see the difference between $m \lessgtr 1/3$ numerically. The thread appears to get depleted even for $m < 1/3$ because of limited numerical precision as L approaches $L_{\max}$. The symptom of a problem is that the depletion time starts depending on the numerical resolution for $m < 1/3$. Of course, the skeins in the hagfish slime do not need to get fully depleted to create the gel, so a power $m < 1/3$ is still applicable. When comparing the different flow scenarios we will explore a range of m and define an 'effective deployment' time $t_{\text{dep},50\%}$, when 50% of the thread length is unravelled.

4.2. Pinned skein

When the skein is pinned and the thread is free at the other end, the tension arises from hydrodynamic drag on the thread. Such a scenario can arise if the skein is arrested in the network of other fibres or in a mucus network.

Consider a free thread ending at $s = 0$ and a pinned skein at $s = L(t)$ (figure 3), so that the Eulerian skein position X is fixed and is thus not a function of time. Unlike the pinned thread case in §4.1, where a shrinking skein led to a decreasing drag, here the tension *increases* with time as the extended thread provides more drag.

We formulate the problem by imposing boundary conditions at the free end, $T_0 = T(0, t) = 0$, and pinned end, $x(L(t), t) = X$. From (3.7) with $T_0 = \dot{X} = 0$ and $T_L = \alpha(\dot{L})^m$, the equation for the growth of the thread is

$$(\dot{L})^m = -4\pi\mu\,\alpha^{-1}L\,\delta(L)\,(\dot{L} + \bar{u}(L, X, t)). \tag{4.10}$$

The slenderness parameter δ depends on L through its definition (3.2). Because the thread extends to the left in figure 3, we must have $\bar{u}(L, X, t) < 0$ to avoid unphysical respooling. The pinned thread equation (4.2) and the pinned skein equation (4.10) have a very similar form, though the drag in the former ($\sim R(L)$) decreases with L and that in the latter ($\sim L\delta(L)$) increases with L.

Using a characteristic velocity U and a characteristic length scale L_0, we obtain the non-dimensional form of (4.10) as

$$(\dot{L}^*)^m = -\wp L^*\delta(L^*)(\bar{u}^*(L^*, X^*, t^*) + \dot{L}^*), \tag{4.11}$$

where $\dot{L}^* = \dot{L}/U$, $L^* = L/L_0$ and $u^*(L^*, t^*) = u(L, t)/U$ are the non-dimensional unravelling rate, unravelled length and flow rate, respectively. The natural dimensionless force ratio (3.14) is

$$\wp = 4\pi\mu\,L_0\,U^{1-m}\,\alpha^{-1}. \tag{4.12}$$

This differs from $\wp$ in (4.4) by replacing R_0 with L_0. It is sensible in this pinned skein case to use the initial thread length L_0, since drag on the thread controls the unravelling rate.

Figure 5 shows a numerical solution of (4.10) for our reference parameter values using a constant velocity field, $u(L, X, t) = -U = -1\ \text{m s}^{-1}$. As before, the lower bound on the depletion time is $L_{\max}/U \approx 167$ ms, and now the

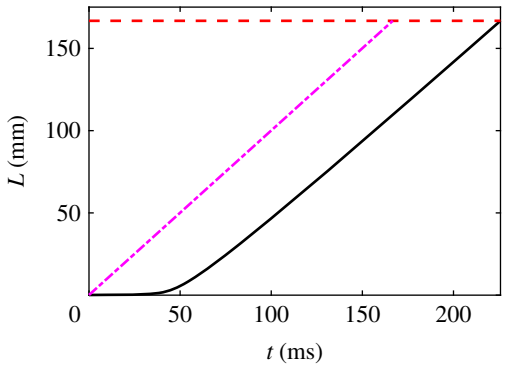

Figure 5. Numerical solution (solid line) of (4.10) for the parameter values $R_0 = 50\ \mu\text{m}$, $L_0 = 2R_0$, $\wp = 1/2$, $m = 1/2$, $U = 1\ \text{m s}^{-1}$. The dashed line (purple) is the upper bound $L = L_0 + Ut$. The horizontal dashed line is at $L = L_{\max}$, when the skein is fully unravelled. Even for such a small force ratio $\wp$ the thread unravels almost as fast as the upper bound. (Online version in colour.)

numerical value is $t_{\text{dep}} \approx 226$ ms. This is slower than what we observed in the pinned thread case ($t_{\text{dep}} \approx 194$ ms), but here we are using the much smaller force ratio $\wp = 1/2$. This shows that the pinned skein case can unravel almost as fast as the lower bound for a much smaller value of $\wp$, since the drag on the thread increases with L, as reflected by the accelerating speed $\dot{L}$ in figure 5. This is in contrast to the deceleration in figure 4 for the pinned thread, where drag decreases as the skein radius diminishes.

4.3. Free skein and thread

In the previous two cases, we took either the thread or skein to be pinned; here we consider the case where neither is pinned, and both are free to move with the flow. This scenario is possible if both the thread and the skein are not stuck to the existing fibrous network, or at the beginning of the slime formation when none of the skeins have unravelled to a significant extent.

The force at the peeling point $x(L(t), t) = X(t)$ is then determined by the balance of two forces: Stokes drag on the spherical skein, $F_1 = 6\pi\mu R\,(u(X, t) - \dot{X})$, and drag on the thread, $F_2 = -4\pi\mu L\delta\,(\dot{L} - \dot{X} + \bar{u}(L, X, t))$. The latter is obtained from (3.7) with $T_L = F_2$ and $T_0 = 0$. Since both the skein and thread are free and we have neglected inertia, $F_1 + F_2 = 0$, which we can use to solve for $\dot{X}$, the velocity of the peeling point in the Eulerian (laboratory) frame. Coupling this with the peel force constitutive model (3.13)–(3.15), the unspooling rate equation is then $\alpha(\dot{L})^m = F_1 = -F_2$. The dynamics of this scenario are governed by the system

$$(\dot{L})^m = -\frac{12\pi\mu\alpha^{-1}RL\delta}{2L\delta + 3R}\,(\dot{L} + \bar{u}(L, X, t) - u(X, t)) \tag{4.13a}$$

and

$$\dot{X} = \frac{2L\delta}{2L\delta + 3R}\,(\dot{L} + \bar{u}(L, X, t)) + \frac{3R}{2L\delta + 3R}\,u(X, t), \tag{4.13b}$$

where $\bar{u}(L, X, t)$ is the thread-averaged velocity (3.8). The velocity (4.13*b*) for the thread–skein system is the average of a velocity $\dot{L} + \bar{u}(L, X, t)$ arising from drag on the thread and a velocity $u(X, t)$ arising from drag on the skein, weighed by the relative strength of the drags.

The difference $\bar{u}(L, X, t) - u(X, t)$ that appears in (4.13*a*) implies that adding a constant to the velocity field does not change the unspooling dynamics, as expected since the thread–skein system is freely advected by the flow, and only relative velocities generate drag. Hence, unlike our previous two cases in §§4.1 and 4.2, a spatially varying flow field is required for unravelling. For a linear velocity field $u(x, t) = \lambda x$, i.e. uniaxial extensional flow with extensional strain rate λ, we have $u(X, t) - \bar{u}(L, X, t) = \lambda L/2$ independent of X, so that we can solve the $\dot{L}$ equation (4.13*a*) by itself,

$$(\dot{L})^m = \frac{6\pi\mu\alpha^{-1}RL}{L + (3R/2\delta)}\left(\frac{1}{2}\lambda L - \dot{L}\right). \tag{4.14}$$

The mass conservation equation (3.10) then relates R to L, and the slenderness parameter (3.2) relates δ to L.

To define a characteristic length scale for this problem, should we use R_0 or L_0 as a length scale? Both are important for the unravelling process to start quickly, but typically L_0 is a bit larger than R_0. A compromise is to use R_0 as the viscous drag length scale and $U = \lambda L_0$ as the velocity scale. The choice of R_0 emphasizes the magnitude of the drag on the skein, and λL_0 reflects the amplitude of velocity gradients over the longer length L_0. We thus obtain the dimensionless form of (4.14) as

$$(\dot{L}^*)^m = \wp\,\frac{R^*L^*}{L^* + (3R^*/2\delta)}\left(\frac{1}{2}L^* - \dot{L}^*\right), \tag{4.15}$$

where $\dot{L}^* = \dot{L}/\lambda L_0$, $R^* = R/R_0$ and $L^* = L/R_0$ are the non-dimensional unravelling rate, skein radius and unravelled length, respectively. The natural dimensionless number in this case is

$$\wp = \frac{6\pi\mu R_0 U}{\alpha U^m} = 6\pi\mu R_0\,(\lambda L_0)^{1-m}\,\alpha^{-1}. \tag{4.16}$$

Assuming as before that $\dot{L} \geq 0$ (the thread does not 'respool'), the right-hand side of (4.14) implies $\dot{L} \leq \lambda L/2$, which gives the constraint that $L(t) \leq L_0\,\text{e}^{(1/2)\lambda t}$. This constraint is the kinematic limit where the thread extends at a rate dictated by the strain rate in the flow. This implies that the depletion time satisfies

$$t_{\text{dep}} \geq 2\lambda^{-1}\log\left(\frac{L_{\max}}{L_0}\right). \tag{4.17}$$

In the two pinned cases we considered before, the lower bound on the depletion time was of the form $t_{\text{dep}} \geq L_{\max}/U$, *independent of* L_0. The lower bound (4.17) depends explicitly on the ratio $L_{\max}/L_0$, so a very short initial thread length will take a long time to unravel, even if $\wp$ is large.

When the thread is almost depleted, the unspooling rate decreases due to the factor of R in (4.14). To see this explicitly, put $L = L_{\max} - U\tau$ in (4.14) and assume τ and $\dot{\tau}$ are small,

$$(-\dot{\tau})^m \approx \frac{1}{2}\wp\left(\frac{U\tau}{L_{\max} - L_0}\right)^{1/3}\frac{L_{\max}}{L_0}, \quad \tau \ll 1. \tag{4.18}$$

This is exactly the same form as (4.6), with a different constant C. We conclude that once again the criterion for finite-time complete unravelling is $m > 1/3$, as it was for the pinned thread case (§4.1). But as before this is not very physically consequential, as it only applies to the last phase of unspooling when the skein is almost completely unravelled.

Figure 6 shows a numerical solution of (4.14) for our reference parameter values and with a strain rate $\lambda = 10\ \text{s}^{-1}$ for $\wp = 10$. (We choose λ such that $\lambda L_{\max}$ is of the same order of magnitude as $U = 1\ \text{m s}^{-1}$ in the pinned cases.) The

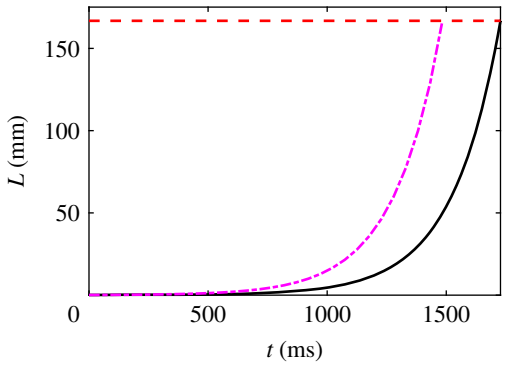

Figure 6. Numerical solution (solid line) of (4.14) for the parameter values $R_0 = 50\ \mu\text{m}$, $L_0 = 2R_0$, $\wp = 10$, $m = 1/2$, $\lambda = 10\ \text{s}^{-1}$. The dashed line (purple) is the upper bound $L_0 \exp(\lambda t/2)$. The horizontal dashed line is at $L_1 = L_{\max}$, when the skein is fully unravelled. (Online version in colour.)

lower bound (4.17) on the depletion time is 1.48 s, and the numerical value is $t_{\text{dep}} \approx 1.73$ s. This is slower than what we observed in the two pinned cases ($t_{\text{dep}} < 1$ s), due to the factor $2\log(L_{\max}/L_0) \approx 14.8$. The slowdown due to the short initial thread length is thus considerable in this case. A longer initial length or a higher strain rate would be needed to make the times comparable.

4.4. Two free skeins (skein splitting)

Another scenario of unravelling is when a skein splits into smaller connected fractions, which then unravel. This scenario is possible since the hagfish ejects the skein through its slime gland and the resulting shear forces (from the ejection process and the fluid's viscous drag) can break the skein into two.

Here we consider the simple case of a skein breaking into two halves. The unravelling may be faster since the initial viscous drag is dominated by two skeins, rather than a skein and a small initial length of thread. A diagram of this configuration is show in figure 7: we model the broken skein as two spheres, of radius R_1 and R_2, respectively, connected by an unravelled length of thread, which can unspool at both ends. We fix a reference point $s = 0$ between the two skeins such that $x(0, t) = X(t)$. The thread then extends a length $L_1(t)$ towards the first skein (right) and $L_2(t)$ towards the second skein (left), with $L = L_1 + L_2$ the total unravelled length. Without loss of generality we take $L_1(0) = L_2(0) = L_0/2$. The peeling force at the first skein ($s = L_1$, $x = X + L_1$) is the sum of the drag forces due to the second skein ($s = -L_2$, $x = X - L_2$) and drag on the thread,

$$T|_{s=L_1} = -6\pi\mu R_2(u(X - L_2, t) - (\dot{X} - \dot{L}_2)) - 4\pi\mu L\delta(\bar{u}(L, X, t) - \dot{X}), \tag{4.19}$$

where now $\bar{u}(L, X, t) := (1/(L_1 + L_2)) \int_{X-L_2}^{X+L_1} u(x, t)\,\mathrm{d}x$. Since the thread and skeins are free, the peeling force at $s = L_1$ (4.19) must balance the viscous drag force on the first skein,

$$T|_{s=L_1} = 6\pi\mu R_1(u(X + L_1, t) - (\dot{X} + \dot{L}_1)). \tag{4.20}$$

Equating (4.19) and (4.20), we can solve for $\dot{X}$,

$$\dot{X} = \frac{3R_1(u(X+L_1,t) - \dot{L}_1) + 3R_2(u(X-L_2,t) + \dot{L}_2) + 2L\delta\bar{u}(L, X, t)}{3(R_1+R_2) + 2L\delta}. \tag{4.21}$$

We use this to eliminate $\dot{X}$ from (4.20),

$$T|_{s=L_1} = \frac{6\pi\mu R_1}{3(R_1+R_2)+2L\delta}(3R_2(u(X+L_1,t) - u(X-L_2,t) - \dot{L}) + 2L\delta(u(X+L_1,t) - \bar{u}(L,X,t) - \dot{L}_1)). \tag{4.22}$$

We can then also carry out the same calculation for the second skein, at $s = -L_2$, and find

$$T|_{s=-L_2} = \frac{6\pi\mu R_2}{3(R_1+R_2)+2L\delta}(3R_1(u(X+L_1,t) - u(X-L_2,t) - \dot{L}) - 2L\delta(u(X+L_2,t) - \bar{u}(L,X,t) + \dot{L}_2)). \tag{4.23}$$

Now it is a matter of solving the coupled peeling equation $\alpha(\dot{L}_1)^m = T|_{s=L_1}$, $\alpha(\dot{L}_2)^m = T|_{s=-L_2}$. To keep things simple, let us take a symmetric configuration centred on $x = X = 0$ where the two skeins are initially of equal size. (Unequal splitting would result in a depletion time in between this case of even splitting and the free skein–thread of §4.3.) We take an antisymmetric velocity field $u(x,t) = -u(-x,t)$ that pulls apart the skeins, such as for an extensional flow $u = \lambda x$. Then $R_1 = R_2$ and $L_1 = L_2$ for all time, and $u = 0$. The tensions (4.22) and (4.23) are then equal and greatly simplify to $T|_{s=L_1} = T|_{s=-L_2} = 6\pi\mu R_1(u(L_1,t) - \dot{L}_1)$. Thus, the dynamics for this case is governed by

$$\alpha(\dot{L}_1)^m = 6\pi\mu R_1(u(L_1,t) - \dot{L}_1). \tag{4.24}$$

The drag force on the thread has dropped out, since the antisymmetric velocity field leads to cancelling forces on the thread. Another way to think of (4.24) is to observe that in making a symmetric configuration, with the two skeins being pulled apart by a straining flow centred on the origin, we have effectively 'pinned' the thread at $x = 0$. We have thus recovered our pinned thread equation (4.2) from §4.1, with the notable difference that now we cannot use a constant velocity field U, but must resort to a straining flow λx or some other non-uniform flow.

We non-dimensionalize (4.24) using a characteristic length scale R_0 and obtain

$$(\dot{L}_1^*)^m = \wp R_1^*(u^*(L_1^*, t^*) - \dot{L}_1^*), \tag{4.25}$$

where $\dot{L}^* = \dot{L}/\lambda R_0$ and $R^* = R/R_0$ are the non-dimensional unravelling rate and skein radius, respectively. The natural dimensionless number in this case is

$$\wp = \frac{6\pi\mu\lambda R_0^2}{\alpha(\lambda R_0)^m} = 6\pi\mu R_0^{2-m}\lambda^{1-m}\alpha^{-1}. \tag{4.26}$$

Figure 8 shows the unravelling dynamics associated with a split skein using parameter values similar to the free configuration of §4.3 and figure 6. The free skein unravels faster when split, as expected (0.756 s versus 1.73 s), owing to a stronger effective drag force and a kinematic upper bound with a rate λ rather than $\lambda/2$. There is an important difference between using the free thread–skein equation (4.13) and the free split-skein equation (4.24): the former has a drag slaved to a short initial thread length, whereas for the latter the drag depends on the initial radius of the split skein, which can easily be larger.

In addition to the four cases discussed in this section, we also analysed a slightly more realistic scenario of suction flow where velocity decays away from the mouth of the predator and we consider a pinned skein at different locations away from the mouth. We use an approximate flow profile from

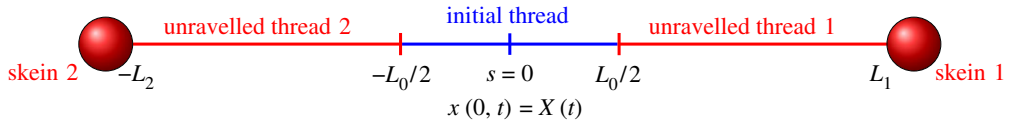

Figure 7. Thread being drawn from two skeins. (Online version in colour.)

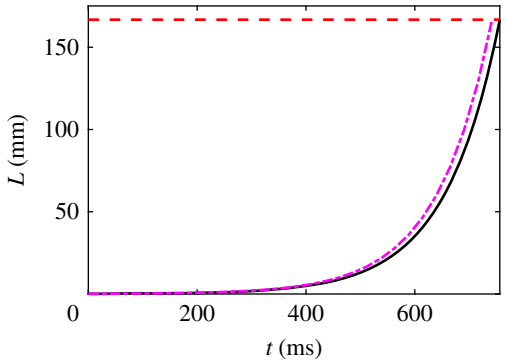

Figure 8. Numerical solution (solid line) for the thread half-length $L_1(t)$ using the force for two symmetric free skeins (equation (4.24)) for the parameter values $R_1(0) = 50\ \mu\text{m}$, $L_1(0) = 2R_1(0)$, $\wp = 10$, $m = 1/2$, $\lambda = 10\ \text{s}^{-1}$. The dashed line (purple) is the upper bound $L_1(0)\exp(\lambda t)$. The horizontal dashed line is at $L_1 = L_{1\max}$, when the skein is fully unravelled. (Online version in colour.)

the experimental data available in the literature (electronic supplementary material, section III). In general, such a flow profile is both spatially and temporally varying, but we neglect time-dependent variations for our analysis. The peak velocity (at the mouth of the predator) was chosen to match the characteristic velocity ($U = 1\ \text{m s}^{-1}$). The velocity decays over a characteristic length scale of the order of the gape size (e.g. opening size of the mouth). We estimate gape size from the video evidence [8] of slime deployment, resulting in extensional strain rates between $0.28–2.2\ \text{s}^{-1}$, with the rate being highest at the predator's mouth. These are smaller extension rates than considered in the earlier cases of this section. The choice of pinning location drastically affects the unravelling time. A depletion time of $\sim$0.4 s was obtained for the case where the skein is pinned at a distance equal to one-third of the gape size of the predator. This is longer than the unravel time we found for the pinned skein in a uniform flow ($\approx$0.22 s), due to the decaying velocity away from the predator's mouth, but the unravelling time still falls close to natural unravelling time scales. More complicated spatially and temporally varying flow fields can be treated in a similar way; we expect the time scales in such cases to be of the order of those we found, given that in real scenarios the thread–skein system can be very close to or in the mouth of the predator, and the non-dimensional quantity $\wp$ is likely to be sufficiently large.

5. Discussion

5.1. The role of the dimensionless parameters $\wp$ and m

The unravelling times for various cases discussed in §4 depend on the dimensionless quantity $\wp$, but also separately on the model parameter m in the peeling force law. This is clear from the dimensionless governing equations in §4 that depend on these two dimensionless parameters separately, although m also appears in the definition of $\wp$. The power-law exponent m determines the peeling force dependence on the unravelling rate. Such a rate dependence exists in peeling scenarios due to the viscoelastic nature of adhesion at the peeling site. In the case of hagfish thread peeling from the skein, the dependence can possibly arise from viscoelastic time scales involved in the deformation of mucous vesicles or the polymeric solution of mucus [15], or the protein adhesive between the loops of thread [11]. The peeling resistance also depends on the dimensional constant factor, α, but its influence on unravelling is built into the dimensionless factor $\wp$, for which $\wp \sim \alpha^{-1}$.

Figure 9 compares all four flow scenarios of §4 as a function of $\wp$ and m in terms of the effective deployment time, i.e. the time to unravel half of the thread length, $t_{\text{dep},50\%}$. (This effective time is used because some flows cannot fully deplete the skein in finite time for $m < 1/3$, as discussed in §4. Moreover, in practice, the threads do not need to be fully unravelled to create slime.) The flow parameters are identical to those previously described. For all cases, the limit of high drag and low peel resistance, $\wp \gg 1$, converges to the kinematic limit of unravelling where unconstrained portions of the skein–thread system exactly advect with the local flow velocity. At the other extreme, viscous drag is weak compared with peel resistance and for some small value of $\wp$ unravelling is too slow to match physiological time scales.

The power-law exponent m is a secondary effect compared with $\wp$. In general, for $\wp > 10$, m has negligible effect on unravelling times. For $\wp < 10$, the dependence on m is case specific. For the cases of pinned thread (§4.1), pinned skein (§4.2) and free skein–thread (§4.3), a larger value of m leads to a smaller unravelling time (while keeping the same value of $\wp$). For the case of skein splitting in an extensional flow (§4.4), such a monotonic trend is not observed and above a critical value of $\wp$ the unravelling is faster for small values of m. This presumably arises from the nonlinearity in the peel force constitutive equation. For example, taking $m = 1$ as a reference case, making $m < 1$ *increases* the dimensionless peel resistance for $\dot{L}^* < 1$, but *decreases* the peel resistance for $\dot{L}^* > 1$. As such, whether the unravelling rate is $\dot{L}^* \gtrless 1$, the exponent m can accelerate or decelerate the unravelling process.

The value of m affects the minimum required $\wp_{\min}$ to achieve unravel times comparable to physiological time scales (i.e. $t_{\text{dep},50\%}$ at or below the dotted lines in figure 9). For the uniform velocity field cases ($U = 1\ \text{m s}^{-1}$), $\wp_{\min}$ is a weaker function of m for the pinned thread case, $\wp_{\min} = 0.29–1.32$, compared with the pinned skein case, $\wp_{\min} = 0.03–3$. For the cases of a free skein–thread in extensional flow, even with splitting, $t_{\text{dep},50\%}$ never falls below 400 ms even at high $\wp$. That is, $t_{\text{dep},50\%}$ is higher than the physiological unravel time scales by a factor of 2 or 3. However, as stated earlier, the time scales in such cases are determined by the specific choice of strain rate, λ, and the initial unravel length L_0. Such kinematic and geometric parameters are certainly variable in reality, and small changes could easily decrease the unravel time scales, as previously discussed.

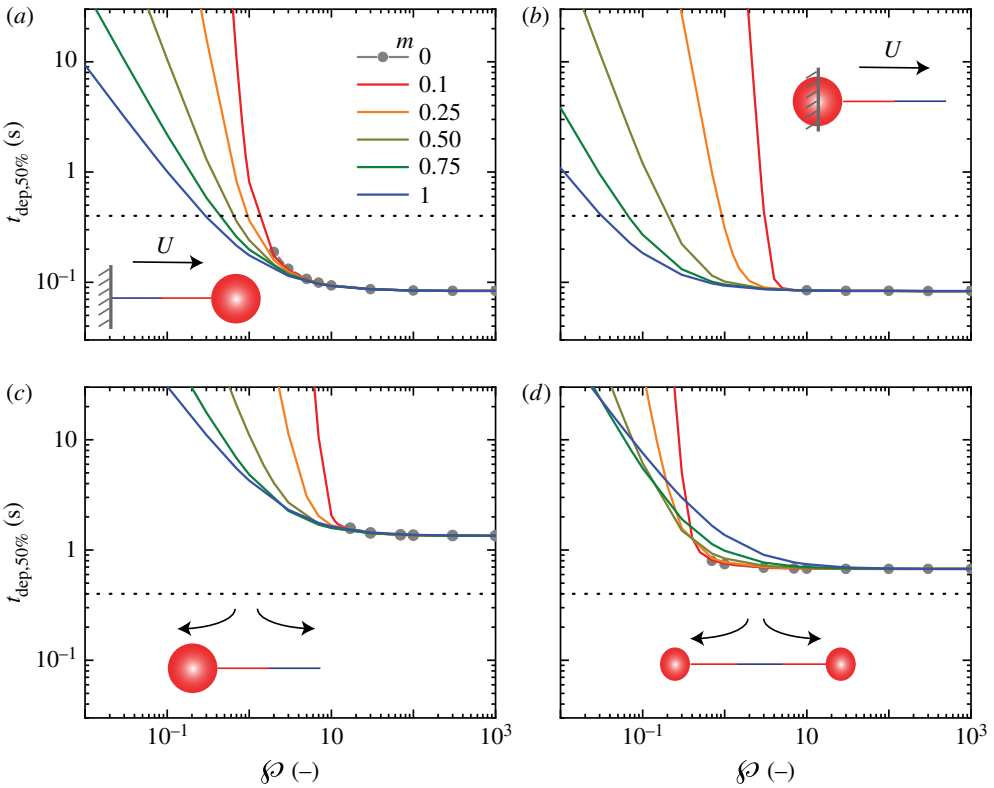

Figure 9. Parameter dependence of 'effective' unravelling. Comparison of time scale $t_{dep,50\%}$ for unravelling half the total length of the fibre for different values of m, as the dimensionless quantity $\wp$ is varied in different unravelling scenarios. (*a*) Pinned thread in uniform flow, (*b*) pinned skein in uniform flow, (*c*) free thread and skein in straining flow and (*d*) symmetric free skeins in straining flow. Other parameters used are $r = 1$ µm, $R_0 = 50$ µm, $L_0 = 2R_0$, $U = 1$ m s^{-1} and $\lambda = 10$ s^{-1}. The dotted horizontal line represents the physiologically observed time scale (=0.4 s). (Online version in colour.)

In any case, m becomes important only when depletion time scales are much larger than the kinematic limit, clearly showing that m is of secondary concern compared with $\wp$.

An important caveat to the $m = 0$ case of $F_P = \alpha =$ constant is that peeling cannot occur ($\dot{L} = 0$) if the viscous drag falls below a critical value. For example, if either the initial skein radius R_0 or thread length L_0 is too small, the viscous drag force is less than F_P and unravelling cannot occur. Thus, in figure 9 a minimum value of $\wp$ is needed for the $m = 0$ cases. The minimum values range from about 1 to 10, depending on the case and the corresponding definition of $\wp$ for the flow and geometry. In three cases, the viscous drag can potentially increase during unravelling as the thread elongates (figure 9*b–d*). In these cases, the minimum $\wp$ is associated with initiating the peeling process. For the other case of the pinned thread, figure 9*a*, the viscous drag decreases during unravelling, since it is slaved to the skein radius, which decreases in size during the process. Unravelling here will eventually stop at a critical value of R. This, therefore, feeds back to requiring a larger critical initial value of $\wp$ to unravel by 50%, and is used in figure 9*a* to determine the domain of $\wp$ for the $m = 0$ case.

5.2. Estimating the parameter $\wp$

A key question remains: what is $\wp$ in physiological scenarios? For this, we must know the peeling force parameters in the constitutive model, and no direct experimental measurements are yet available. Here we make estimates for the two extreme conditions of $m = 1$ and $m = 0$, i.e. a linear dependence on velocity (akin to a constant viscous damping coefficient) and a constant peel force, respectively.

For the $m = 1$ case, we consider viscous resistance acting at the peel site with stress $\sigma = \mu_u \dot{\epsilon}$, where μ_u is the uniaxial extensional viscosity between the separating thread and the skein (related to shear viscosity as $\mu_u = 3\mu$), and $\dot{\epsilon} = \dot{L}/L_c$ is the local extensional strain rate that depends on the peel velocity $\dot{L}$ and the characteristic velocity gradient length L_c. The stress acts over the characteristic thread–thread contact area, which we assume scales as $A \approx d^2$, i.e. contact across the diameter and the length of contact along the thread also scales with the diameter. The peel force is then

$$F_P \approx \mu_u \left(\frac{\dot{L}}{L_c}\right) d^2. \tag{5.1}$$

Comparing with the peeling law in (3.15), $F_P = \alpha \dot{L}^m$, we get

$$\alpha = \mu_u \frac{d^2}{L_c}; \quad m = 1. \tag{5.2}$$

Substituting this into $\wp = F_D/F_P$, and considering the majority of cases where drag is set by the skein radius R_0, i.e. equations (4.4), (4.16), (4.26), we obtain

$$\wp = \frac{6\pi\mu R_0 U}{\mu_u(\dot{L}/L_c)d^2} = 6\pi \frac{\mu}{\mu_u} \frac{U}{\dot{L}} \frac{R_0 L_c}{d^2}, \tag{5.3}$$

where important ratios have been grouped. The simplest case is peel viscosity arising from the surrounding viscous liquid at the peel site. In other words, the viscosity causing drag is also resisting peeling, and to cast in terms of extensional viscosity we take $\mu_u = 3\mu$, a result for a Newtonian fluid. The viscosity μ may be that of sea water, or a surrounding mucous vesicle solution with higher viscosity, but under

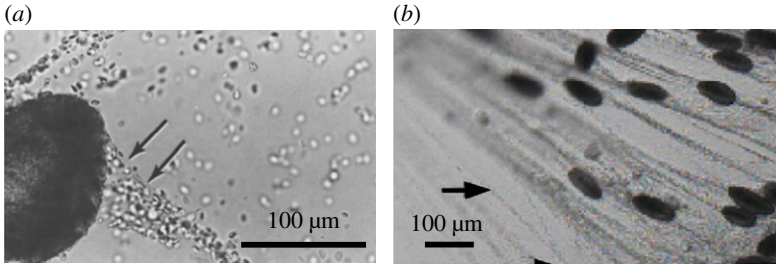

Figure 10. (*a*) Mucous vesicles aggregating on unravelling thread (adapted from Koch *et al.* [21]). (*b*) Mucous vesicles aggregated on unravelling thread elongated along with the fibre under the flow (adapted from Winegard & Fudge [22]).

these assumptions the ratio μ/μ_u is still the same. Furthermore, typically $U/\dot{L} \gtrsim 1$, and the velocity gradient length scale is likely set by the thread radius, $L_c \approx r$. Then (5.3) dramatically simplifies to

$$\wp = 2\pi \frac{R_0}{d}, \tag{5.4}$$

which clearly estimates $\wp \gg 1$, or more specifically for $R_0 = 50\ \mu\text{m}$ and $d = 2\ \mu\text{m}$, $\wp \approx 160$. If drag is instead dominated by the thread length L_0, e.g. for the pinned skein case of §4.2, then the numerator in (5.3) would be modified by replacing $6\pi R_0$ with $4\pi L_0$. We expect L_0 to be of the same order as R_0, e.g. a single curl in the coil. But if L_0 is smaller, it would decrease $\wp$ accordingly.

Our specific assumptions can modify the details, but in general we estimate that physiological conditions for $m = 1$ would give $\wp > 1$, if not $\wp \gg 1$. The velocity gradient length scale L_c could be smaller than the thread radius r. A decrease in L_c/r makes $\wp$ proportionally smaller, but it is difficult to imagine this being more dramatic than, say, a factor of 10. The velocity ratio $U/\dot{L}$, if anything, will be larger than 1, and this proportionally increases the estimate of $\wp$. The viscosity ratio μ/μ_u could be smaller, e.g. if the viscosity of proteins between thread wrappings is larger than the surrounding viscous liquid. However, we note that the surrounding viscous liquid can have a very large viscosity, e.g. the measured extensional viscosity of hagfish mucous vesicle solutions obtained by Böni *et al.* [15] is $\mu_u \approx 10\ \text{Pa s}$. This is much higher than water, $\mu_u \approx 3\ \text{mPa s}$. An additional mechanism of increasing drag, and $\wp$, is for mucous vesicles to bind on the thread during the unravelling process (figure 10), which would transmit additional forces to the drag term, as suggested by Winegard & Fudge [22]. Such a scenario is possible since mucous vesicles and thread cells are densely packed inside the slime glands and are released simultaneously. For all of these variations, $\wp > 1$ seems very likely for physiological conditions in this constant viscosity estimate for $m = 1$.

To estimate physiological $\wp$ for $m = 0$, the other extreme of a constant force resisting peel, we consider peel strength interactions between the skein fibres solely due to van der Waals forces. We estimate $F_P = \alpha \approx 10^{-7}\ \text{N}$ (see electronic supplementary material, section II). Substituting into $\wp = F_D/F_P$, and considering cases where drag is set by the skein radius, i.e. equations (4.4), (4.16), (4.26), with $R_0 = 50\ \mu\text{m}$, water viscosity $\mu = 1\ \text{mPa s}$, and $U = 1\ \text{m s}^{-1}$, gives $\wp \approx 90$. We see that $\wp \gg 1$ with these assumptions. Even if the force resisting peeling is larger by a factor of 10 or 100, still $\wp \gtrsim 1$ and viscous hydrodynamics can provide rapid unravelling that can be very close to the kinematically derived lower bounds on unravelling time.

6. Conclusion

Our analysis shows that, under reasonable physiological conditions, unravelling due to viscous drag can occur within a few hundred milliseconds and is accelerated if the skein is pinned at a surface, such as the mouth of a predator. A dimensionless ratio of viscous drag to peeling resistance, $\wp = F_D/F_P$, appears in the dynamical equations and is the primary factor determining unravelling time scales. Large $\wp$ corresponds to fast unravelling that approaches a kinematic limit wherein free portions of the thread–skein system directly advect with the local flow velocity. For characteristic velocity U, the bound is $t_{dep} \geq L_{max}/U$, whereas for extensional flows with strain rate λ, $t_{dep} \geq \lambda^{-1} \log(L_{max}/L_0)$, where L_0 is the initial thread length.

The modelling approach captures essential features and insights by considering a single skein unravelling in idealized flow fields. Future modelling efforts could build on our work by expanding and detailing several aspects, primarily with new experimental measurements of peel strength for skein unravelling, but also details of physiological flow fields including characteristic velocities and strain rates. Real physiological scenarios are more complex due to chaotic flows and multi-body interactions (multiple skeins, mucous vesicles). Our model does not consider such interactions, or the important feature of unravelled threads interacting to create a network. At leading order, we expect such modelling to require more complex flow fields that create extension (to unravel fibres) but also bring different fibres together. Mixing flows would be excellent candidates for theoretical analysis, and any experimental characterization of physiological flow fields should keep this perspective in mind, e.g. simple suction flow with extension, but no mixing, may not be sufficient to create a network of unravelled threads.

Although the physiological flow fields may be different from the ones that were used in the analysis, our results underline the importance of viscous hydrodynamics and boundary conditions on the process. Recent work [11] found that Pacific hagfish skeins undergo spontaneous unravelling in salt solution. However, the observed unravelling time scales (∼min) are much larger than the physiological time scales (approx. 0.4 s) during the attack. It is possible that ion transport to the peeling site may help in peeling the adhesive contacts, which may be diffusion limited without flow. Although it is known that flow is required to accelerate unravelling to $t_{dep,50\%} < 1\ \text{s}$, it is not yet clear whether flow-enhanced ion transport may also contribute to a faster unravelling, in addition to the drag effects. The effects of various salt ions on the swelling and rupture of mucin vesciles have been studied in the past [18,19], but the influence of such ionic effects on the skeins and their deployment is not yet known. If ion transport and chemistry are important, this would modify the F_P behaviour and require

modelling of transport at the peel site due to flow. Our results do not rule out the possibility of ion-mediated unravelling but provide an alternative mechanism of unravelling which may be occurring alone or in conjunction with a multitude of other processes.

Data accessibility. The Matlab code used in the article for various numerical solutions is available at https://github.com/jeanluct/hagfish-unravel.

Authors' contributions. J.-L.T. and R.H.E. conceived the study. G.C., R.H.E. and J.-L.T. performed the analysis and wrote the paper.

Competing interests. We declare we have no competing interests.

Funding. This work is supported by the 10.13039/501100008982 National Science Foundation under grant no. CBET-1342408.

Acknowledgements. We thank Prof. Douglas S. Fudge (Chapman University, CA, USA) for providing the hagfish exudate and for many helpful discussions.

References

1. Bishop KL, Wainwright PC, Holzman R. 2008 Anterior-to-posterior wave of buccal expansion in suction feeding fishes is critical for optimizing fluid flow velocity profile. *J. R. Soc. Interface* **5**, 1309–1316. (doi:10.1098/rsif.2008.0017)
2. Yaniv S, Elad D, Holzman R. 2014 Suction feeding across fish life stages: flow dynamics from larvae to adults and implications for prey capture. *J. Exp. Biol.* **217**, 3748–3757. (doi:10.1242/jeb.104331)
3. Chapman JW, Klaassen RHG, Drake VA, Fossette S, Hays GC, Metcalfe JD, Reynolds AM, Reynolds DR, Alerstam T. 2011 Animal orientation strategies for movement in flows. *Curr. Biol.* **21**, R861–R870. (doi:10.1016/j.cub.2011.08.014)
4. Oteiza P, Odstrcil I, Lauder G, Portugues R, Engert F. 2017 A novel mechanism for mechanosensory-based rheotaxis in larval zebrafish. *Nature* **547**, 445–448. (doi:10.1038/nature23014)
5. Waggett RJ, Buskey EJ. 2006 Calanoid copepod escape behavior in response to a visual predator. *Mar. Biol.* **150**, 599–607. (doi:10.1007/s00227-006-0384-3)
6. Downing S, Salo W, Spitzer R, Koch E. 1981 The hagfish slime gland: a model system for studying the biology of mucus. *Science* **214**, 1143–1145. (doi:10.1126/science.7302586)
7. Fudge DS, Levy N, Chiu S, Gosline JM. 2005 Composition, morphology and mechanics of hagfish slime. *J. Exp. Biol.* **208**, 4613–4625. (doi:10.1242/jeb.01963)
8. Zintzen V, Roberts CD, Anderson MJ, Stewart AL, Struthers CD, Harvey ES. 2011 Hagfish slime as a defence mechanism against gill-breathing predators. *Sci. Rep.* **1**, 131. (doi:10.1038/srep00131)
9. Jørgensen JM, Lomholt JP, Weber RE, Malte H. 1998 *The biology of hagfishes*. London, UK: Chapman & Hall.
10. Fernholm B. 1981 Thread cells from the slime glands of hagfish (Myxinidae). *Acta Zool.* **62**, 137–145. (doi:10.1111/azo.1981.62.issue-3)
11. Bernards MA, Oke I, Heyland A, Fudge DS. 2014 Spontaneous unraveling of hagfish slime thread skeins is mediated by a seawater-soluble protein adhesive. *J. Exp. Biol.* **217**, 1263–1268. (doi:10.1242/jeb.096909)
12. Lim J, Fudge DS, Levy N, Gosline JM. 2006 Hagfish slime ecomechanics: testing the gill-clogging hypothesis. *J. Exp. Biol.* **209**, 702–710. (doi:10.1242/jeb.02067)
13. Ewoldt RH, Winegard TM, Fudge DS. 2011 Non-linear viscoelasticity of hagfish slime. *Int. J. Non-Linear Mech.* **46**, 627–636. (doi:10.1016/j.ijnonlinmec.2010.10.003)
14. Winegard T *et al.* 2014 Coiling and maturation of a high-performance fibre in hagfish slime gland thread cells. *Nat. Commun.* **5**, 3534. (doi:10.1038/ncomms4534)
15. Böni L, Fischer P, Böcker L, Kuster S, Rühs PA. 2016 Hagfish slime and mucin flow properties and their implications for defense. *Sci. Rep.* **6**, 30371. (doi:10.1038/srep30371)
16. Böni LJ, Zurflüh R., Baumgartner ME, Windhab EJ, Fischer P, Kuster S, Rühs PA. 2018 Effect of ionic strength and seawater cations on hagfish slime formation. *Sci. Rep.* **8**, 9867. (doi:10.1038/s41598-018-27975-0)
17. Chaudhary G, Fudge DS, Macias-Rodriguez B, Ewoldt RH. 2018 Concentration-independent mechanics and structure of hagfish slime. *Acta Biomater.* **79**, 123–134. (doi:10.1016/j.actbio.2018.08.022)
18. Herr JE, Winegard TM, O'Donnell MJ, Yancey PH, Fudge DS. 2010 Stabilization and swelling of hagfish slime mucin vesicles. *J. Exp. Biol.* **213**, 1092–1099. (doi:10.1242/jeb.038992)
19. Herr JE, Clifford AM, Goss GG, Fudge DS. 2014 Defensive slime formation in pacific hagfish requires Ca^{2+} and aquaporin mediated swelling of released mucin vesicles. *J. Exp. Biol.* **217**, 2288–2296. (doi:10.1242/jeb.101584)
20. Newby WW. 1946 The slime glands and thread cells of the hagfish, Polistrotrema stouti. *J. Morphol.* **78**, 397–409. (doi:10.1002/(ISSN)1097-4687)
21. Koch EA, Spitzer RH, Pithawalla RB, Downing SW. 1991 Keratin-like components of gland thread cells modulate the properties of mucus from hagfish (*Eptatretus stouti*). *Cell Tissue Res.* **264**, 79–86. (doi:10.1007/BF00305724)
22. Winegard TM, Fudge DS. 2010 Deployment of hagfish slime thread skeins requires the transmission of mixing forces via mucin strands. *J. Exp. Biol.* **213**, 1235–1240. (doi:10.1242/jeb.038075)
23. Tornberg AK, Shelley MJ. 2004 Simulating the dynamics and interactions of flexible fibers in Stokes flows. *J. Comput. Phys.* **196**, 8–40. (doi:10.1016/j.jcp.2003.10.017)
24. Hong DC, Yue S. 1995 Deterministic chaos in failure dynamics: dynamics of peeling of adhesive tape. *Phys. Rev. Lett.* **74**, 254–257. (doi:10.1103/PhysRevLett.74.254)
25. Cortet PP, Ciccotti M, Vanel L. 2007 Imaging the stick-slip peeling of an adhesive tape under a constant load. *J. Stat. Mech.* **2007**, P03005. (doi:10.1088/1742-5468/2007/03/P03005)
26. Mohammed IK, Charalambides MN, Kinloch AJ. 2016 Modeling the effect of rate and geometry on peeling and tack of pressure-sensitive adhesives. *J. Non-Newtonian Fluid Mech.* **233**, 85–94. (doi:10.1016/j.jnnfm.2016.01.016)
27. Liu Z, Lu H, Zheng Y, Tao D, Meng Y, Tian Y. 2018 Transient adhesion in a non-fully detached contact. *Sci. Rep.* **8**, 6147. (doi:10.1038/s41598-018-24587-6)
28. Dalbe MJ, Santucci S, Cortet PP, Vanel L. 2014 Strong dynamical effects during stick-slip adhesive peeling. *Soft Matter* **10**, 132–138. (doi:10.1039/C3SM51918J)
29. Wang Z, Wang Z, Dai Z, Gorb S. 2018 Bio-inspired adhesive footpad for legged robot climbing under reduced gravity: multiple toes facilitate stable attachment. *Appl. Sci.* **8**, 114. (doi:10.3390/app8010114)
30. De R, Maybhate A, Ananthakrishna G. 2004 Dynamics of stick-slip in peeling of an adhesive tape. *Phys. Rev. E* **70**, 046223. (doi:10.1103/PhysRevE.70.046223)
31. Griffin MA, Engler AJ, Barber TA, Healy KE, Sweeney HL, Discher DE. 2004 Patterning, prestress, and peeling dynamics of myocytes. *Biophys. J.* **86**, 1209–1222. (doi:10.1016/S0006-3495(04)74195-8)